Fluid–membrane interaction based on the material point method

Allen R. York II[1,*,†], Deborah Sulsky[2] and Howard L. Schreyer[3]

[1]*Advanced Modeling and Software Systems Group, Applied Research Associates, 811 Spring Forest Road, Raleigh, NC 27609, U.S.A.*
[2]*Department of Mathematics and Statistics, University of New Mexico, Albuquerque, NM 87131, U.S.A.*
[3]*Department of Mechanical Engineering, University of New Mexico, Albuquerque, NM 87131, U.S.A.*

SUMMARY

The material point method (MPM) uses unconnected, Lagrangian, material points to discretize solids, fluids or membranes. All variables in the solution of the continuum equations are associated with these points; so, for example, they carry mass, velocity, stress and strain. A background Eulerian mesh is used to solve the momentum equation. Data mapped from the material points are used to initialize variables on the background mesh. In the case of multiple materials, the stress from each material contributes to forces at nearby mesh points, so the solution of the momentum equation includes all materials. The mesh solution then updates the material point values. This simple algorithm treats all materials in a uniform way, avoids complicated mesh construction and automatically applies a noslip contact algorithm at no additional cost. Several examples are used to demonstrate the method, including simulation of a pressurized membrane and the impact of a probe with a pre-inflated airbag. Copyright © 2000 John Wiley & Sons, Ltd.

KEY WORDS: material point method; gridless; meshless; fluid–structure

1. INTRODUCTION

Fluid-membrane systems are quite common and include parachutes, vehicle airbags, high-speed magnetic tapes, printing presses, inflatable structures, pressure transducers, blood vessels, and bladder tanks. These systems are especially difficult to model numerically when the structural response is non-trivial (e.g. not rigid) and, in turn, has an effect on the fluid. A typical method of achieving fluid–membrane or, more generally, fluid–structure simulation is to couple a fluids code with a structures code [1–5]. The procedure involves embedding a Lagrangian structure in an

---

*Correspondence to: Allen R. York II, Applied Research Associates, Inc., 811 Spring Forest Road, Suite 100, Raleigh, NC 27609, U.S.A.
†E-mail: ayork@sed.ara.com

Copyright © 2000 John Wiley & Sons, Ltd.

Eulerian mesh used to calculate the fluid dynamics. The intersection of the structure and the Eulerian mesh is calculated, and the appropriate boundary conditions are imposed on each mesh. The necessity of defining the intersection of the two meshes usually accounts for a significant amount of the analysis run time. Also, large differences in the wave speed of the fluid and solid may lead to inefficiency in explicit codes unless special techniques are used to cycle one material domain multiple timesteps during a single timestep of the other.

Arbitrary Lagrangian–Eulerian (ALE) methods have also been used for fluid–structure interaction [6–14]. In the ALE method the mesh can have an arbitrary velocity. In many cases it is convenient to pick the structure mesh velocity to be the material velocity and transition the mesh associated with the fluid from Lagrangian close to the structure to Eulerian far from the structure. This method generally affords a less complicated approach to describing the fluid–structure interface than the coupling of separate codes, but the meshes and their motion must be chosen carefully for good performance.

Particle, element-free, and meshless methods have been receiving considerable attention recently, as evidenced by special issues of journals [15, 16]. One such method is the material point method (MPM). The MPM has evolved from a particle-in-cell (PIC) method called FLIP originally developed at Los Alamos National Laboratory for fluid dynamics problems [8, 9]. The basic formulation of the MPM has been described by Sulsky *et al.* [10–12] which also show applications to materials having strength and stiffness. This paper describes an extension of the method to model the interaction of fluids and membranes. The MPM for membranes alone has been previously described by York *et al.* [13].

With MPM, a mesh of Lagrangian material points is used to discretize one or more solid bodies, membranes or fluid. The material points have mass and velocity and carry stress and strain, which may be history dependent. The interaction of the material points is calculated on a background Eulerian or spatial finite element mesh on which the momentum equation is solved. Material point quantities are updated from the solution on the Eulerian mesh with mapping functions.

The advantages of both Lagrangian and Eulerian methods are realized in the MPM. Mesh distortion and entanglement are not a problem as it might be with Lagrangian schemes since the background mesh is under user control and can be redefined each time step if desired. Advection of history-dependent variables is straightforward since the variables are defined on material points which themselves advect through the Eulerian mesh. Thus, numerical dissipation normally associated with an Eulerian method is avoided.

The advancement reported here is the straightforward treatment of the interaction between the surfaces of the fluid and the membrane which is done with a simple algorithm. Buijk [2] reports that most of the CPU time for a fluid–structure simulation is used to determine the intersection of the Lagrangian membrane elements and the Eulerian elements.This step is avoided when using the MPM for fluid–structure interaction calculations. Material points, solid and fluid, carry stress. The stress results in internal forces at nearby grid nodes. The momentum equation is solved at the grid nodes taking into account the internal forces from all nearby materials. On boundaries between the fluid and the structure, the internal forces in mixed solid–fluid elements determine the interface conditions. Materials within the same computational element at a given timestep will see the same increment in strain, but can have different stress because each material point follows its own constitutive equation.

The basic ideas presented here are somewhat similar to the immersed boundary method used by Peskin in simulating blood flow through the human heart [17, 18] and the related immersed

interface method of LeVeque and Li [19]. Peskin immerses massless Lagrangian points, chained together to form the heart surface, in an incompressible fluid. The fluid is represented only on an Eulerian mesh. As with our method, the Lagrangian points do not have to coincide with the grid node points of the mesh. Forces from their connected neighbours are computed at each Lagrangian point and interpolated to the mesh to provide constraints on the fluid motion in fluid–structure interactions. The points then move in the computed velocity field. Instead of interpolating forces to the grid, LeVeque and Li use the position of the interface, given by the connected Lagrangian points, to alter the finite difference scheme by incorporating jump conditions at the interface in order to derive a second-order accurate method [19]. In the MPM both the structure and the fluid are represented by unconnected Lagrangian points that are treated the same with the exception of constitutive relations that relate stress to strain or strain rate.

There are several advantages inherent to the MPM for simulation of fluid–structure interaction. The time step constraint for the explicit method is a function of the mesh size and not of the spacing between material points. There has been no additional restriction observed in the time step when performing calculations with fluids and structures as has been reported in some methods [20–22]. No-slip contact is automatic and is provided at no additional computational cost. Meshing is also simplified over many methods since all that is required is unconnected points placed on a membrane surface or placed to fill a volume of fluid or solid. The background mesh does not have to conform to surfaces, and surfaces do not have to be meshed in the usual way.

The governing and discrete equations for solids have been discussed previously [10–12]. These equations and the additional equations necessary for the simulation of compressible, viscous fluids are reviewed in Section 2. The methodology for the fluid–membrane coupling is presented in Section 3 along with the constitutive relations for solids, membranes, and compressible fluids. To date, only elastic membranes have been simulated. The theory in these sections is presented in general, however the numerical examples, included in Section 4, are performed with a two-dimensional implementation of the method. First, a fluid-only, shock-tube problem is presented as a test of the algorithm for compressible fluids. Next, three examples of simulations involving fluid–membrane interaction are discussed. A one-dimensional piston-container problem tests the interaction of fluid and solid in the MPM. A more stringent, two-dimensional test is presented next, where a pressurized membrane with complicated geometry is allowed to expand to its equilibrium circular shape. The last example is a simulation of a probe impacting an inflated airbag where comparison is made of the MPM results, a similar finite element calculation and experiments. Finally, concluding comments are presented in the last section.

2. EQUATIONS OF MOTION

Motion of a continuum is governed by conservation of mass, momentum and energy. A region of fluid or a solid body occupies a volume Ω_0 initially and Ω_t at later times. (Membranes occupy a surface rather than a volume.) For the current position $\mathbf{x} \in \Omega_t$ at time t, let $\rho(\mathbf{x}, t)$ be the mass density, $v(x, t)$ be the velocity, $\sigma(\mathbf{x}, t)$ be the Cauchy stress tensor, and $b(x, t)$ be the specific body force in the current configuration. The conservation of mass equation is

$$\dot{\rho} = -\nabla\rho \cdot \mathbf{v} \tag{1}$$

where the superposed dot represents the material time derivative, and $\nabla(\ )$ is the gradient with respect to the current configuration. Conservation of linear momentum is given by

$$\nabla \cdot \sigma + \rho \mathbf{b} = \rho \mathbf{a} \tag{2}$$

in which $\mathbf{a} = \dot{\mathbf{v}}$ is the acceleration. Finally, conservation of energy can be written

$$\rho \dot{e} = \sigma : \dot{\varepsilon} \tag{3}$$

with e being the specific internal energy and

$$\dot{\varepsilon} = \tfrac{1}{2}[(\nabla \mathbf{v} + (\nabla \mathbf{v})^{\mathrm{T}}] \tag{4}$$

denoting the strain rate. Fluids and solids are distinguished by the constitutive equation relating the stress to strain or strain rate. Specific constitutive models will be given in the next section. Initial conditions and boundary values complete the specification of the continuum problem.

In the material point method, the material in Ω_0 is discretized by dividing it up into material elements, a material point is placed in each element, and the point is assigned a mass based on the volume of the element and the initial material density (Figure 1). The mass assigned to a material point is kept fixed throughout the computation, insuring global mass conservation. Other initial properties of the material, like velocity, stress, strain or energy are also assigned to the material points, as appropriate for a given problem. Instead of solving the equations of motion on the material point mesh, the momentum equation is solved on a background Eulerian mesh, chosen to cover the domain Ω_t. This background mesh provides a convenient means to define discrete derivatives, and keeps the computational work linear in the number of material points. The source data for the solution of the momentum equation on the Eulerian mesh come from the material points.

2.1. Spatial discretization of the governing equations

In the following development all variables with a subscript i or j reference grid values, and variables with subscript p-represent material point values. Equation (2) can be discretized as
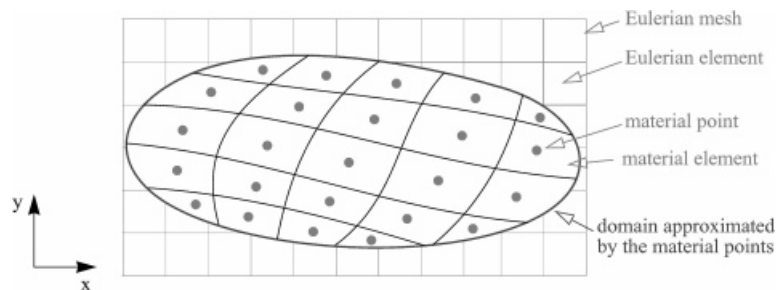

Figure 1. Mesh of Lagrangian material points representing the domain of interest overlaid on the computational mesh.

described previously [10–12] which results in a governing equation at each grid node of the Eulerian mesh. This equation takes the form

$$\sum_{j=1}^{N_n} m_{ij}\mathbf{a}_j = \mathbf{f}_i^{\text{int}} + \mathbf{f}_i^{\text{ext}}, \quad i = 1,\ldots,N_n \tag{5}$$

where m_{ij} is the consistent mass matrix, $\mathbf{a}_j$ is the acceleration at node j, $\mathbf{f}_i^{\text{int}}$ and $\mathbf{f}_i^{\text{ext}}$ are the internal and external forces at node i, and N_n is the number of grid nodes. To define the mass matrix, introduce nodal basis functions $N_i(\mathbf{x})$, then the mass matrix is

$$m_{ij} = \sum_{p=1}^{N_p} m_p N_i(\mathbf{x}_p)N_j(\mathbf{x}_p) \tag{6}$$

where m_p is the mass of material point p and N_p is the total number of material points. In this work, the mapping $N_i(\mathbf{x})$ is given by bilinear nodal basis functions used routinely in the finite element method. The consistent mass matrix is replaced by the diagonal form simplifying Equation (5) at the expense of introducing a slight amount of numerical dissipation [23] to give

$$m_i\mathbf{a}_i = \mathbf{f}_i^{\text{int}} + \mathbf{f}_i^{\text{ext}}, \quad i = 1,\ldots,N_n \tag{7}$$

where the diagonal components of the mass matrix are

$$m_i = \sum_p m_p N_i(\mathbf{x}_p), \quad i = 1,\ldots,N_n \tag{8}$$

Equation (7) can be recast into momentum form as

$$\frac{\mathrm{d}\mathbf{p}_i}{\mathrm{d}t} = \mathbf{f}_i^{\text{int}} + \mathbf{f}_i^{\text{ext}}, \quad i = 1,\ldots,N_n \tag{9}$$

where $\mathbf{p}_i = m_i\mathbf{v}_i$ is the momentum, and i ranges from one to the number of grid nodes. The external forces are problem specific and are handled as in many methods. The internal forces are computed from the divergence of the stress; an explicit formula is given below.

2.2. Time-integration algorithm

The discrete equations are to be solved at a discrete set of time steps, t^k, $k = 1,\ldots,K$. The superscript k indicates an approximation at time level k so that, for example, m_i^k is the approximation to $m_i(t^k)$. The momentum equation is solved using an updated Lagrangian frame. If we use an explicit integration of Equation (9) to find the change in momentum, $\Delta\mathbf{p}_i$, the momentum for node i at the end of the Lagrangian step is

$$\mathbf{p}_i^L = \mathbf{p}_i^k + \Delta\mathbf{p}_i = \mathbf{p}_i^k + \Delta t(\mathbf{f}_i^{\text{int},k} + \mathbf{f}_i^{\text{ext},k}) \tag{10}$$

where $\Delta t = t^{k+1} - t^k$. Note that the grid mass, m_i^k, depends on time due to the movement of material points through the grid; however, through the Lagrangian step defined in Equation (10) the grid mass is constant. The momentum, $\mathbf{p}_i^k$, in Equation (10) is determined from a mass-weighted mapping of material point velocities, $\mathbf{v}_p^k$, to the grid nodes

$$m_i^k \mathbf{v}_i^k = \sum_{p=1}^{N_p} m_p^k \mathbf{v}_p^k N_i(\mathbf{x}_p^k) \tag{11}$$

The material point velocity and position are updated using typical finite element nodal basis functions that map the grid node values of velocity and acceleration to the material points

$$\mathbf{v}_p^{k+1} = \mathbf{v}_p^k + \sum_{i=1}^{N_n} \Delta \mathbf{p}_i N_i(\mathbf{x}_p^k)/m_i^k$$

$$\mathbf{x}_p^{k+1} = \mathbf{x}_p^k + \sum_{i=1}^{N_n} \Delta t \, \mathbf{p}_i^L N_i(\mathbf{x}_p^k)/m_i^k \tag{12}$$

The strain increment $\Delta \varepsilon_p$ at a material point is computed from the grid node velocities

$$\Delta \varepsilon_p^{k+1} = \frac{\Delta t}{2} \sum_{i=1}^{N_n} \left[G_{ip}^k \mathbf{v}_i^{k+1} + (G_{ip}^k \mathbf{v}_i^{k+1})^{\mathrm{T}} \right] \tag{13}$$

where

$$G_{ip}^k \mathbf{v}_i^{k+1} = \nabla(\mathbf{v}_i^{k+1} N_i(\mathbf{x}))|_{x=x_p^k} \tag{14}$$

is the gradient of the grid velocity evaluated at $\mathbf{x}_p$, and the grid velocity $\mathbf{v}_i^{k+1}$ is determined using Equation (11). Care must be taken in evaluating Equation (14) to include the spatial variation of the basis vectors, for example in using axisymmetric cylindrical co-ordinates in two-dimensions [12]. The strain increment for the material point is used in the constitutive model to update the material point stress. Constitutive equations are discussed in the next section.

The material point stresses are combined directly to compute the internal forces at the grid nodes. The gradient of the nodal basis function, G_{ip}^k, yields the stress divergence

$$\mathbf{f}_i^{\mathrm{int},k} = -\sum_p \frac{m_p}{\rho_p^k} G_{ip}^k \sigma_p^k \tag{15}$$

where the quotient of material point mass and density, m_p/ρ_p^k, is the volume of material point p, and σ_p^k is the stress at material point p. The value of ρ_p^k is updated from the continuity equation

$$\rho_p^{k+1} = \rho_p^k/(1 + \mathrm{tr}\,(\Delta \varepsilon_p^{k+1})) \tag{16}$$

where tr is the trace.

3. FLUID–MEMBRANE INTERACTION

It is proposed that fluid–structure interaction problems be simulated with the MPM. The idea is straightforward in that the coupled problem is set-up as any other type of MPM simulation. The difference is that some material points are designated structure or membrane material points and others are designated fluid material points. The initial mass of membrane material points is determined from the input membrane density (mass per unit area), the input membrane thickness and the user-specified point spacing. The effect of the fluid on the structure and vice versa will be determined on the grid when the momentum equation is solved at each grid node. The coupling of the fluid and structure is indirect in the sense that the pressure from a fluid material point is not directly applied to the neighbouring structure material points. Instead, the forces from fluid and solid material points are calculated together at grid nodes where the divergence of the material point stress is summed.

Equation (17) and Figure 2 symbolically show accumulation of the grid forces from fluid (subscript 'f') and membrane (subscript 'm') material points

$$\mathbf{f}_i \propto \sum_f (\nabla \cdot \sigma_f) V_{f,p} + \sum_m (\nabla \cdot \sigma_m) V_{m,p} \qquad (17)$$

using the fluid and membrane stresses, σ_f and σ_m, and the respective material point volumes, $V_{f,p}$ and $V_{m,p}$.

The net effect of the force summation is that the grid forces cause accelerations of neighbouring fluid and structure material points. The velocity of the interface of the fluid and structure is the same, and there is no penetration of the fluid into the structure. This no-slip feature is automatic since Equation (12) moves the material points in a continuous velocity field obtained by solving the momentum equation. The continuity of the velocity field implies that material points at the same location move together. There is also no penetration, even with discrete time steps, if the usual Lagrangian time step condition is satisfied, that an element not fold during the step. Since
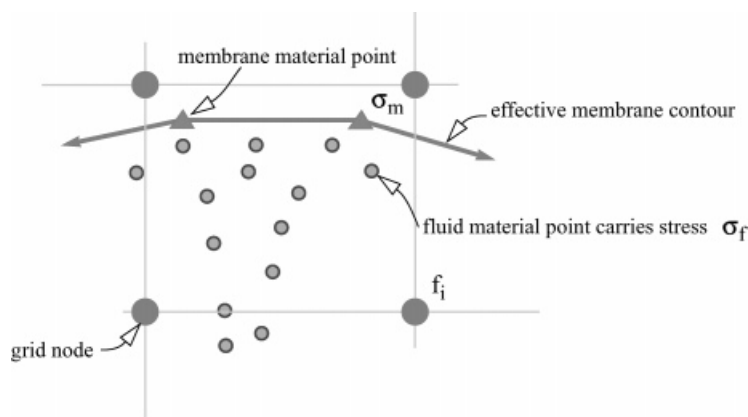

Figure 2. Fluid–structure coupling.

the mesh is under user control, this is almost never a limiting condition. For example, in this paper every step is started from a square mesh. For a slip condition on the boundary special measures must be taken. Similar treatments have been made to account for friction conditions between materials in the context of solid mechanics and, in principle, can apply to fluid–solid interfaces [24]. Slip conditions are not addressed in this paper.

Since Lagrangian material points are used for both the fluid and the structure and since the two are indirectly coupled, the time-consuming calculations involved in defining the interface and applying the correct boundary conditions are avoided. Also, mixed elements are handled naturally as the material points carry material properties with them. The following sections discuss the various constitutive equations applied to the material points.

3.1. Solid constitutive equation

The mechanical response of solids can be quite varied, from elastic to plastic to viscoelastic or viscoplastic. Any of these responses can be implemented in the MPM framework. For example, the constitutive equation for an elastic or inelastic solid can be written in rate form as

$$\overset{\triangledown}{\sigma} = \mathbf{T} : \dot{\varepsilon} \tag{18}$$

where the strain rate, $\dot{\varepsilon}(\mathbf{x}, t)$, is the symmetric part of the velocity gradient given in Equation (4), and $\mathbf{T}$ is the tangent modulus tensor. In all the simulations reported here, T is the conventional fourth-order elasticity tensor since only materials with linear elastic properties are considered. The left-hand side of Equation (18) denotes an objective stress rate; the Jaumann rate is used in this work since it is easy to implement and the strains are not that large. The existing approach in the MPM for solid materials is to calculate the strain increment $\Delta\varepsilon_p$ at a material point from the grid node velocities, according to Equation (13). The stress at a material point is updated by discretizing Equation (18) in a frame indifferent formulation. For the Jaumann rate

$$\sigma_p^{k+1} = \sigma_p^k + \Delta t(\sigma_p^k \cdot \mathbf{W}_p^k - \mathbf{W}_p^k \cdot \sigma_p^k) + T : \Delta\varepsilon_p^{k+1} \tag{19}$$

where the vorticity is

$$\mathbf{W}_p^k = \frac{1}{2} \sum_{i=1}^{N_n} (G_{ip}^k \mathbf{v}_i^{k+1} - (G_{ip}^k \mathbf{v}_i^{k+1})^{\mathrm{T}}) \tag{20}$$

The use of the tangent modulus in the constitutive equation is meant to be symbolic. For inelastic models, the total strain increment, $\Delta\varepsilon_p$, is input into a subroutine that determines the appropriate split into elastic and plastic parts and the resulting stress increment [11]. If the constitutive model contains path-dependent internal variables, these can be assigned to the material points and also integrated in time, as necessary.

3.2. Membrane constitutive equation

A membrane is a thin structure that has no bending resistance and constant traction through its thickness. The membrane is represented in the MPM by individual material points which

collectively define a membrane surface. Figure 3 illustrates the concept in two dimensions. Figure 3(a) shows a planar membrane contour and Figure 3(b) shows a material point discretization of the membrane. The material points are overlaid on the Eulerian mesh. A single layer of material points is used through the thickness of the membrane so the enforcement of constant traction through the thickness is automatic. The membrane formulation in the MPM has been described previously in Reference [13].

Recall that the momentum equation is being solved at the nodes of the Eulerian mesh. Thus, the motion of the material points resulting from the solution of the momentum equation on the grid must be consistent with the forces in the membrane and the geometry of the membrane. This consistency is obtained by projecting the strain increment calculated for each material point (Equation (13)) onto the local co-ordinate system of the membrane. This local system is defined in two dimensions by the normal and tangent vectors, n_p and t_p (Figure 4). The local co-ordinate system is determined using the numbering sequence of the membrane points. The points are numbered consecutively along the membrane contour, and thus, neighbour points are easily determined. With the neighbour points known, an approximation to the tangent and normal directions to the membrane can be made.

In three dimensions, as with other methods, the membrane surface could be meshed, and the connectivity of material points (nodes) on the mesh used to determine the local normal and tangential co-ordinate system. Research is currently underway to eliminate the need for ordered numbering of material points. The local co-ordinate system can be determined by defining the membrane surface as an isosurface of a scalar function. The gradient of the surface function results in the surface normal. Some promising results have been obtained, and will be reported in a later paper.

After the tangent strain has been updated using the local co-ordinate system, the determination of stress for a material point with linear elastic properties is straightforward. For example, if a uniaxial membrane or string is assumed, this projection results in a stress component tangent to the surface of the membrane, with all other components zero. The out-of-plane strains can be adjusted to give either a uniaxial stress or plane stress formulation. The stresses are projected back to the global co-ordinate system for the evaluation of internal forces (Equation (15)) which are defined at grid nodes.
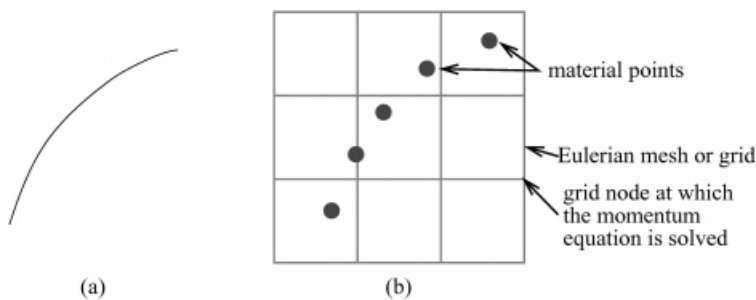

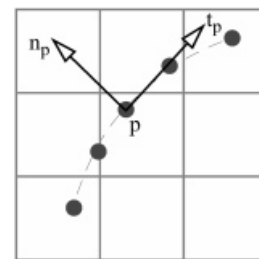Figure 3. (a) Physical membrane contour; and (b) material point representation.

Figure 4. Local 2D co-ordinate system for a material point on the membrane.

3.3. Fluid constitutive equation

Here we give the specific constitutive equation and energy equation used to simulate problems involving compressible fluids. The stress tensor for a fluid point is given as

$$\sigma = 2\mu\dot{\varepsilon} - \tfrac{2}{3}\mu \operatorname{tr}(\dot{\varepsilon})\mathbf{I} - \hat{p}\mathbf{I} \tag{21}$$

where $\mathbf{I}$ is the second-order unit tensor, μ is shear viscosity, $\dot{\varepsilon}$ is the strain-rate tensor and $\hat{p}$ is pressure which is determined from an equation-of-state. Equation (21) assumes the Stokes condition $\lambda = -(\tfrac{1}{2})\mu$ where λ is bulk viscosity, and as a result, the static pressure (spherical component of stress) is equal to the thermodynamic pressure.

To implement the fluid model, Equation (21) is applied at the material points. The strain rate for a material point is computed by dividing Equation (13) by the time step. The equation of state is for a polytropic gas where pressure, $\hat{p}$, is related to density and internal energy by

$$\hat{p} = (\gamma - 1)\rho e \tag{22}$$

where e is specific internal energy, and γ is the ratio of specific heats. The equation is applied at each material point with density of a material point, ρ_p, updated according to the continuity equation (16). The contribution of the fluid stress to the internal force at a grid node is computed in the same way as for a solid or membrane point (Equation (15)). The equation of state (22) is dependent upon internal energy as well as density. Thus, the internal energy is updated for each fluid material point every time step

$$e_p^{k+1} = e_p^k + \sigma_p^{k+1}\Delta\dot{\varepsilon}_p^{k+1}/\rho_p^{k+1} \tag{23}$$

It is well known that most numerical simulations of compressible-fluid shocks provide more accurate results if some type of artificial viscosity is used at the shock front. The artificial viscosity implemented in the MPM is similar to that described by Wilkins [25]. An additional term, q, is added to the material point pressure under shock conditions as

$$q = (\sqrt{c_{\max}^2 g})\,\rho\tilde{\lambda}D\left[c_1 + \frac{c_2|\nabla\cdot\mathbf{v}|}{\max|\nabla\cdot\mathbf{v}|}\right] \tag{24}$$

where

$$D = \begin{cases} \nabla\cdot\mathbf{v} & \nabla\cdot\mathbf{v} < 0 \\ 0 & \nabla\cdot\mathbf{v} > 0 \end{cases} \tag{25}$$

and $c_{\max}^2$ is the maximum sound speed in the fluid, g is a geometric constant proportional to the mesh size, $\tilde{\lambda}$ is an artificial bulk modulus, ρ is density, and c_1 and c_2 are constants. The variable D defined in Equation (25) forces the artificial pressure q to be zero unless the material point is in compression. Note that the divergence of the velocity is the trace of the strain-rate tensor.

4. NUMERICAL EXAMPLES

Sample simulations of the MPM membrane–fluid interaction model are presented in this section. First, a fluid-only, shock-tube problem demonstrates the algorithm for compressible fluids. Next, three examples of simulations involving fluid–membrane interaction are discussed. A one-dimensional piston-container problem tests the interaction of fluid and solid in the MPM. A more stringent, two-dimensional test is presented next, where a pressurized, gas-filled membrane with complicated geometry is allowed to expand to its equilibrium circular shape. The last example is a simulation of a probe impacting an inflated airbag where comparison is made of the MPM results, a similar finite element calculation and experiments.

4.1. Simulation of shock propagation in a fluid (Sod's problem)

The objective of the simulation is to test the implementation of the MPM fluid formulation with a problem that has an analytical solution. Sod investigated finite difference schemes for simulation of a shock propagating through fluids [26]. Sod's model problem consists of a shock tube where a diaphragm separates two regions which have different densities and pressures. Initially, the regions have zero velocity. At time $t = 0$, the diaphragm is broken. Figure 5 (top) illustrates the initial conditions of the problem. The shock strength is defined as the ratio of p_2/p_1 where p_2 and p_1 are the pressures on either side of the shock. For this problem the shock strength is approximately 3.0, which gives a shock speed of about 1.75. The shock is allowed to travel a distance of 0.25, which it should do in 0.143 s. This is a one-dimensional problem, however, it is solved with the MPM in two dimensions, and the solution variables are constant with respect to the y (vertical) direction. A square background grid is used with 200×1 square elements of
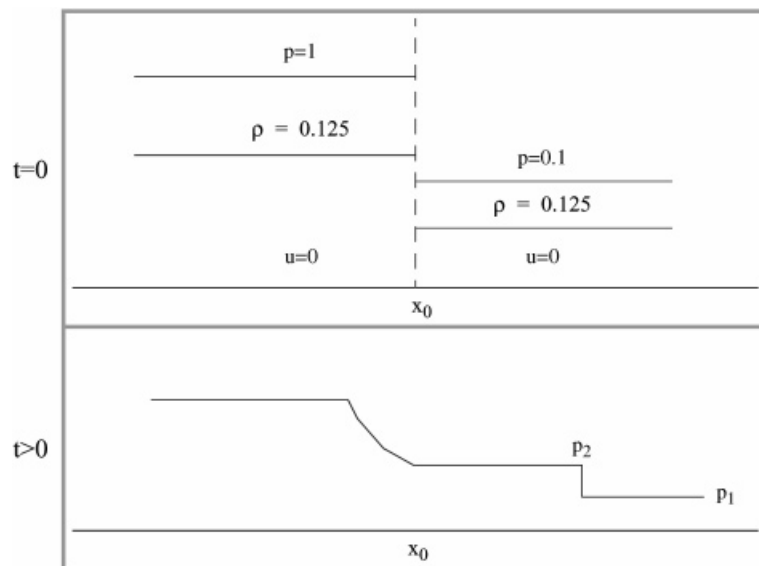

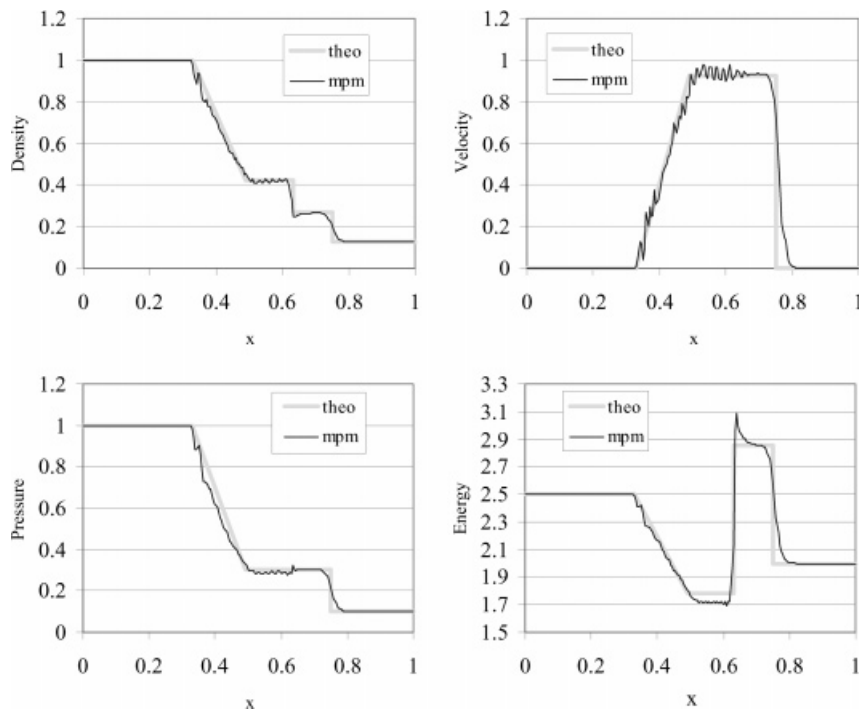Figure 5. Sod's fluid shock propagation problem.

Figure 6. Results of Sod's problem simulation with the MPM.

dimension 0.005, and three material points are initially placed in each element, for a total of 600 material points.

The results of the MPM simulations are shown in Figure 6 with thin dark lines, and the theoretical values are shown with thick grey lines. The simulation is performed with artificial viscosity which smooths the oscillations at the shock front, but also smears the shock slightly. The parameters for the artificial viscosity are, $g = \sqrt{2}\,\mathrm{d}x$, $\tilde{\lambda} = 0.75$, and $c_1 = c_2 = 1$, where $\mathrm{d}x$ is the length of a side of an element. All data are calculated and plotted at grid vertices except density which is plotted at element centres. More sophisticated shock capturing methods would provide sharper shocks; however, this simple approach suffices to illustrate the capability of the MPM to simulate compressible fluids. Shocks are not a significant feature in the remaining fluid–structure interaction problems discussed below.

4.2. Piston-container problem

The piston-container problem is a relatively simple one-dimensional problem. The objective of this simulation is to test the fluid–structure interaction algorithm on a simple scale using a test problem with a known solution.

An illustration of the piston-container fluid–structure problem is shown in Figure 7, and the ideal MPM representation is shown in Figure 8. Since the problem is one dimensional the membrane does not bend, and thus, resists compression the same manner as it resists tension.
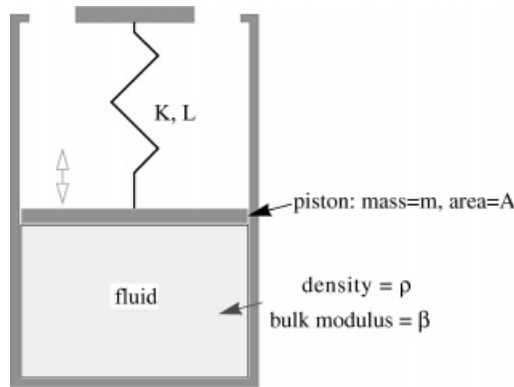
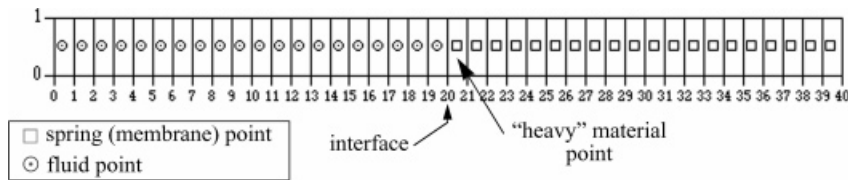Figure 7. Piston-container problem.

Figure 8. Piston-container MPM simulation set-up.

The interaction between the fluid and structure (spring) occurs only at the single interface between the differing materials. At this interface, the fluid and structure stresses contribute internal forces for the solution of the momentum equation. A similar fluid–structure problem is presented by Olson [27].

A massless spring of constant K and length L is attached to a piston. The piston can move without friction to compress or expand a compressible fluid of density ρ and bulk modulus β. The objective is to compare the theoretical frequency of vibration with that from an MPM simulation.

The fluid is assumed to be compressible, inviscid, and adiabatic. The continuity, energy, and constitutive relations combine to give the relationship between pressure and displacement as follows:

$$p = -\beta(\nabla \cdot \mathbf{U}) \tag{26}$$

where U is displacement and β is the isentropic bulk modulus. The analytical expression for the natural frequency, ω, of vibration of the mass satisfies the equation

$$\omega - \sqrt{[K + \rho\omega c A \cot(\omega L/c)]/m} = 0 \tag{27}$$

where c is the wave speed $\sqrt{\beta/\rho}$, m is the piston mass, and A is the piston cross-sectional area.

The parameters used in the MPM simulation are as follows: $L = 20$, $A = 1.0$, $K = 100$, $\rho = 0.0001$, $\beta = 1.58 \times 10^6$, and m variable. The spring is modelled with a linear elastic

constitutive model so that it also has resistance in compression. The points making up the one-dimensional membrane or spring have a small mass compared to the heavy material point at its end, which has a mass 100 times that of other material points. To determine the frequency of vibration, the heavy material point representing the piston is given a small initial velocity, and the position of this material point is monitored.

The first solution of Equation (27) gives the fundamental mode of vibration. Table I lists the theoretical natural frequency and period for two different piston masses along with the period observed in the MPM simulation. The observed periods are very close to the theoretical ones. Figure 9 shows the time history of displacement of the mass. The vertical dashed lines in the plot represent the theoretical periods of vibration.

4.3. Membrane expansion

A membrane with an arbitrary initial configuration and a fluid with an initial pressure will evolve, with viscous dissipation, to an equilibrium shape of a sphere or a circle in two dimensions. Here

Table I. Piston-container periods of vibration.

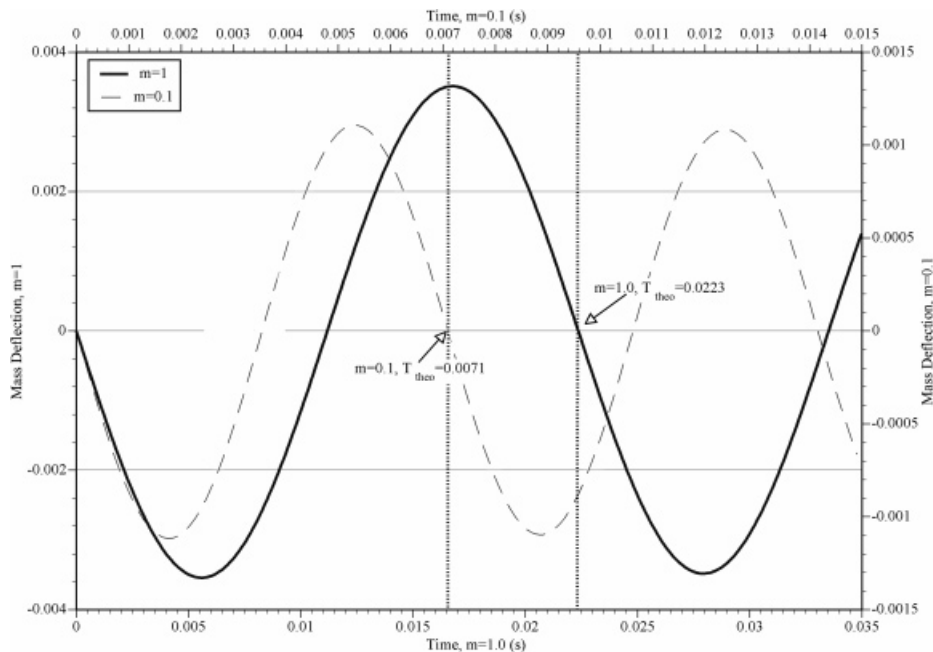| Mass, m	Theoretical ω (rad/s)	Theoretical period (s)	MPM simulation period (s)
0.1	886.2	0.00709	0.0071
1.0	281.2	0.02234	0.022

Figure 9. Mass (Piston) deflection in the piston-container simulations.

an initial dog-bone shape has been chosen as a severe test for the MPM. The dog-bone-to-cylinder membrane expansion simulation is an arbitrary problem (not seen in the literature) that tests several aspects of fluid–structure interaction. The initial conditions for the problem are shown in Figure 10, and the problem parameters are listed in Table II. A computational element size of 0.1 is shown in the figure; a total of four different element sizes were used.

The problem consists of a gas under internal pressure which expands filling a cavity that is initially dog-bone shaped. A membrane forms the cavity and confines the gas. At early times, the membrane oscillates due to unbalanced forces. Since the fluid is given a non-zero viscosity coefficient, the membrane oscillations are damped until a steady-state condition is reached.

There are several areas where this problem can be compared to theory. Some of these are as follows:

(1) the gas should not escape from the membrane,
(2) the equilibrium shape of the membrane should be circular,
(3) the stress in the membrane should be consistent with the internal pressure.

Table III lists some of the results of the four simulations that were performed. The simulations are more refined going from 1 to 4 as indicated by the element or mesh size in the second column. Square elements are used. The last two columns show the final average pressure and average radius of the membrane. The final radius of the membrane appears to converge with mesh
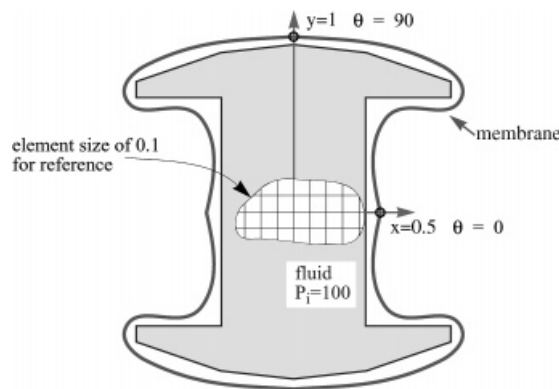

Figure 10. Initial conditions for the dog-bone membrane expansion simulation.

Table II. Fluid and membrane properties.

Fluid property	Value	Membrane property	Value
Density	1.0	density	0.5
Viscosity, μ	0.2	Young's modulus	1×10^6
Initial specific internal energy, i	250	Poisson's ratio, v	0.3
Ratio of specific heats, γ	1.4		
Artificial viscosity	off		

Table III. Membrane expansion simulation parameters
and results.

Simulation	element size	Final radius*	Final internal pressure*
1	0.4	1.07	50.3
2	0.2	1.33	28.8
3	0.1	1.35	31.2
4	0.05	1.36	31.7

*Calculated by averaging values at material points.

Table IV. Comparison of hoop stress.

Simulation	Hoop stress*	Hoop stress-simulation[†]	% Difference
1	539	101	− 81.3
2	385	399	3.6
3	420	400	− 4.8
4	443	433	− 2.3

* Hoop stress, pr/t, is calculated using the final radius and pressure from
Table III with thickness equal to 0.1.
[†] Average of material point membrane stress.

refinement as does the final internal pressure. The higher final pressures of the more refined simulations are consistent with less energy dissipation observed in the plots of the total energy.

Table IV is a comparison of the theoretical hoop stress with the hoop stress observed in the simulations. The theoretical stress is calculated with the final radius and pressure from Table III. There is roughly a 2–5 per cent difference between the theoretical value and the simulation value, neglecting the overly coarse simulation. One source of error arises from the fact that the forces are calculated at grid nodes, and the radius used for the hoop stress calculation in the first column is based on material point locations.

Figures 11–13 illustrate the detailed results of the most coarse and most refined membrane expansion simulations. For each simulation, the material point positions during the initial oscillations are shown along with the shape at steady state. Following this is a plot of the membrane radius as a function of time, measured at 0 and 90° from the horizontal axis, and a plot of the energy.

4.3.1. Simulation 1. Simulation 1 is the coarsest simulation with an element size of 0.4. Figure 11 shows the material point locations at increasing times. The simulation is so coarse that the folds or wrinkles in the membrane cannot be pulled out to a circular shape at equilibrium. However, it can be seen that gas does not escape the membrane and that the membrane shape does move toward a circular shape although the circular shape is not achieved.

Time-history plots of the radius at 0 and 90° show that the radii differ by 0.2 at the steady state, corresponding to the noncircular shape in Figure 11. The time history is also somewhat noisy.
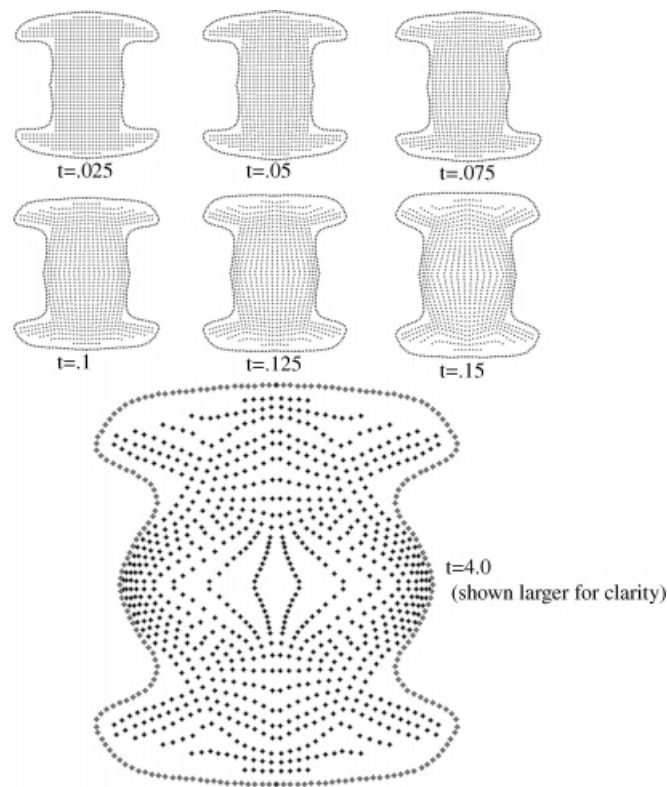
Figure 11. Material point position plots for simulation 1.

Kinetic energy and potential energy for both the fluid and the membrane are also monitored, as well as the total energy. On the coarse mesh, about 1.5 per cent of the total energy is lost due to numerical dissipation. The trends observed during mesh refinement are: (i) the final shape of the membrane becomes more circular, (ii) oscillations during the approach to steady state are smoother, and (iii) there is less energy dissipation.

4.3.2. Simulation 4. Figure 12 shows the material point locations at increasing times for the simulation with the highest resolution (mesh size 0.05). The final time ($t = 4$) is shown larger for clarity. The membrane lines are smooth, and the general shape is approximately the same as in the simulation with mesh size 0.01 (not shown). The same applies to the radii and energy as seen in Figure 13. There is a 0.03 per cent increase in the total energy during the simulation, and the oscillations in the radii are smooth and are converging to the same value, indicating a final circular shape.

4.4. Airbag impact simulation

Axisymmetric calculations of a cylindrical probe impacting an inflated airbag were performed and reported by de Coo [28]. The calculations were compared to experimental results.
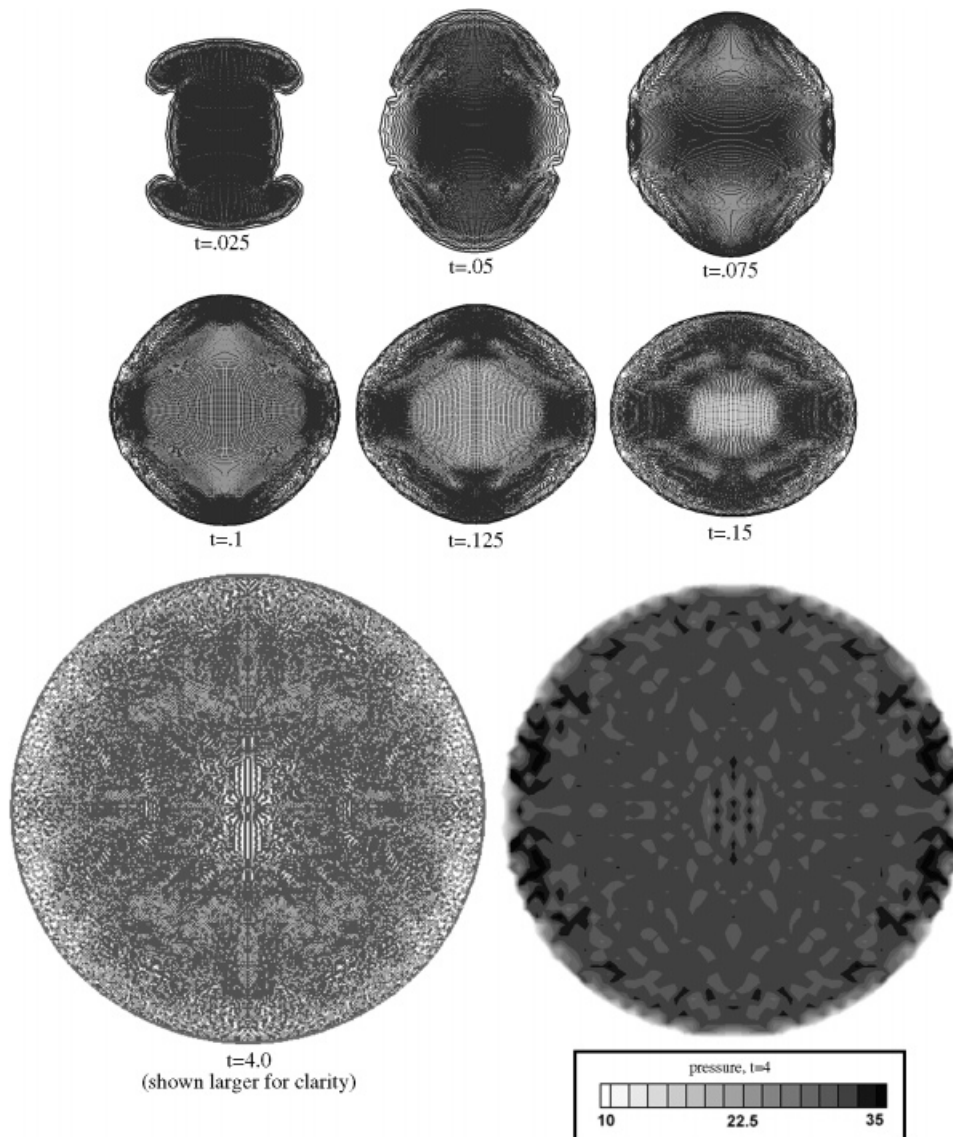
Figure 12. Material point position plots and pressure contours for simulation 4.

A schematic of the problem is shown in Figure 14. The horizontal axis at the bottom of the figure is a symmetry axis for cylindrical coordinates. The MPM is used to simulate one of the experiments reported by de Coo where the diameter, mass, and impact velocity of the cylindrical probe were varied. The parameters of the simulation are listed in Table V. Material properties for the simulation are listed in Table VI.
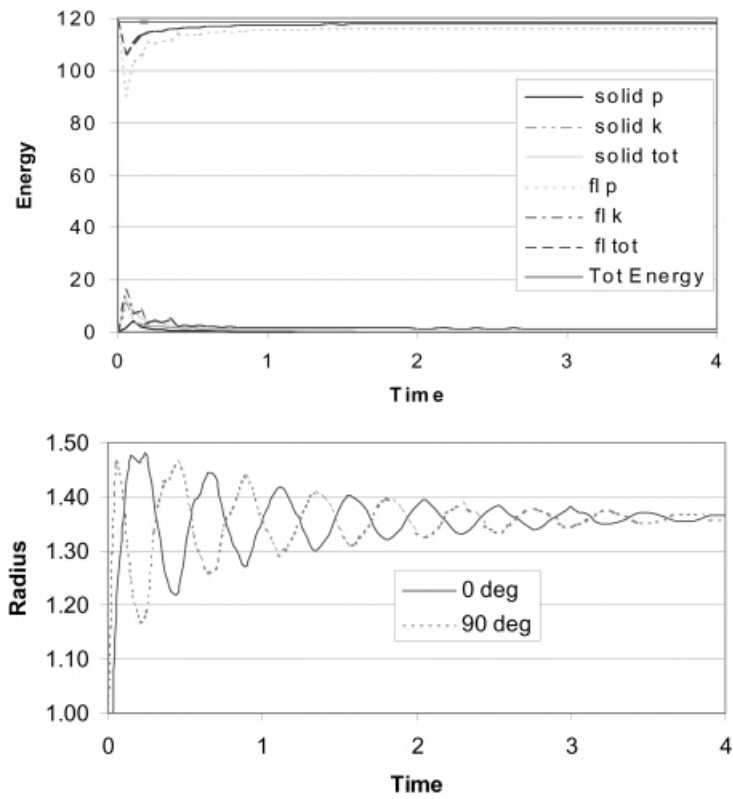
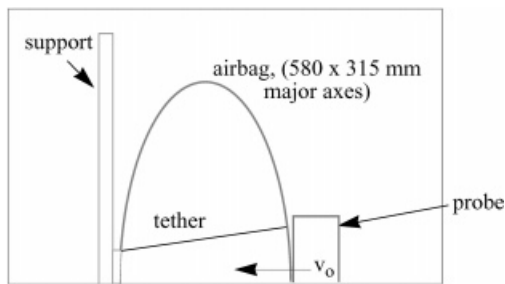Figure 13. Radii and energy for membrane expansion simulation 4.
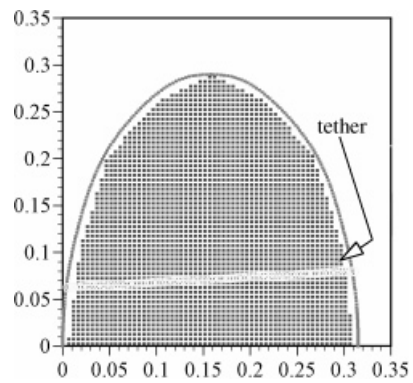

Figure 14. Airbag impact problem.

Figure 15. Initial configuration with the internal tether.

Table V. Airbag impact simulation parameters.

Cylinder (probe) diameter (mm)	Cylinder mass (kg)	Cylinder initial velocity (m/s)
200	6.03	3.90

Table VI. Airbag impact simulation—material properties.

Airbag property	Value	Air property	Value
Thickness	0.5 mm	Specific heat ratio	1.4
Density	662 kg/m3	Density	1.2156 kg/m^3
Young's modulus	$6 \times 10^7 \text{ N/m}^2$	Initial pressure	4000 N/m^2
Poisson's ratio	0.4	Initial specific internal energy	8226 J/kg

Material properties of the cylinder were not listed. Therefore, Young's modulus was arbitrarily chosen to be $5 \times 10^7 \text{ N/m}^2$, and the density was adjusted to give the correct mass. The total airbag mass was derived to be 367.2 g.

The initial positions of the membrane material points for this simulation were arrived at by conducting a simulation with a tether in the airbag. The initial positions of the material points are shown in Figure 15. This configuration was allowed to come to approximate equilibrium and the resulting airbag shape was used as the initial shape for the simulation of the probe impact. The objective of this exercise was to obtain an initial shape that matches that reported by de Coo.

The plots of the probe and airbag material point positions for various times during the simulation are shown in Figure 16. The effect of using the tether to determine initial material point positions is seen in the first plot of Figure 16. The tether pulled the material to the left (indicated by the arrow in the top left plot).

For the simulation with the probe, the tether was removed at the instant the simulation was started because in the axisymmetric MPM calculation this tether is actually a conical shape and affects the flow of the gas material points. There were approximately 3000 material points representing the gas. These are not shown in Figure 16 to increase the clarity of the airbag shape. The predicted configuration of the airbag and impactor look plausible. As the impactor moves to the left, it depresses the airbag, causing the airbag to bulge out in response. The probe slows after impact, eventually stops and then rebounds to the right.

Figure 17 shows a comparison of the displacement of the probe into the airbag for the MPM simulation, the PISCES simulation and the experiment [28]. Figure 18 shows that the deformed airbag shapes at $t = 40$ ms are similar. The slope of the displacement past the peak in Figure 17 differs from that displayed by the experimental data. It is thought that the effect of not simulating the tether may cause a more rapid rebound of the impactor since the airbag expansion is not restrained. To test this theory, a simulation was conducted where the tether was left in the simulation for the duration. It was observed that the slope past the peak closely matched that of the experiment, which did incorporate a tether. However, the cylinder displaced about 20 mm farther into the airbag. This excessive displacement is attributed to the interference of the tether with the gas flow.
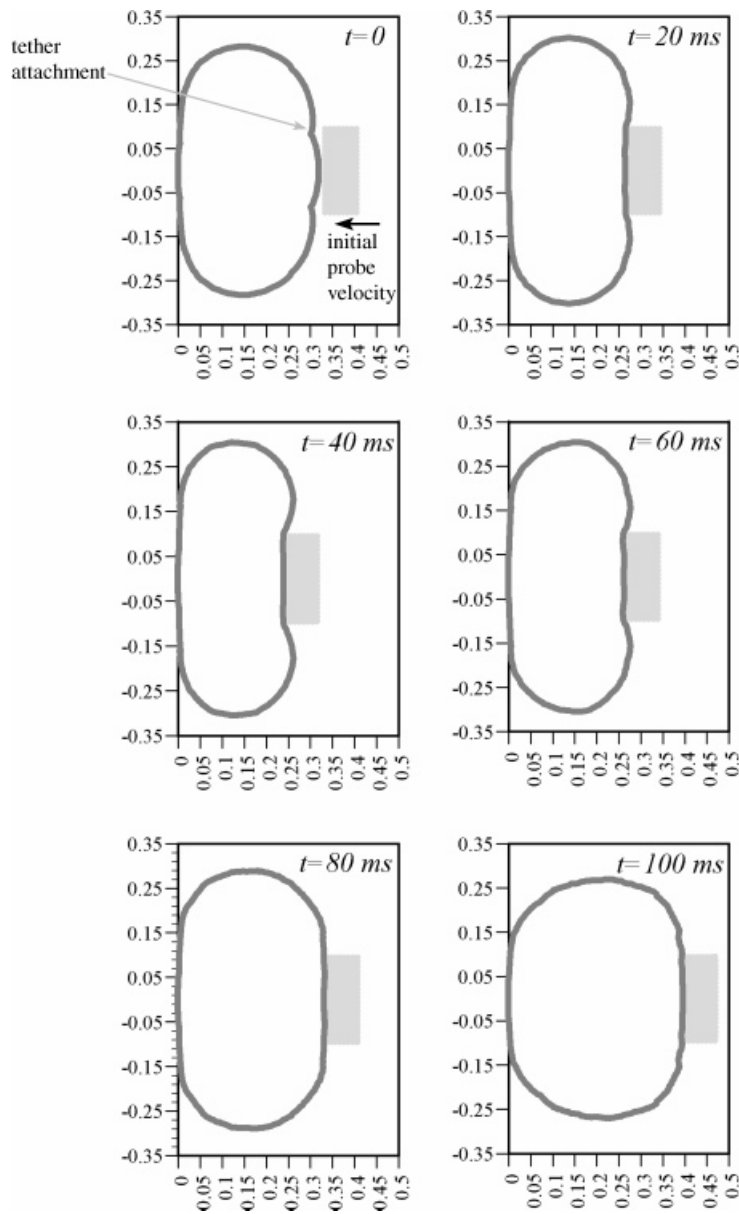
Figure 16. Deformed airbag shapes.

An alternative to modelling the tether with material points would be to prescribe a force–displacement relationship between two material points. The force–displacement relationship could be that of a spring or bar to represent the tether, but in general could take any form. This force would be interpolated to the grid at the two particle locations and included as an external
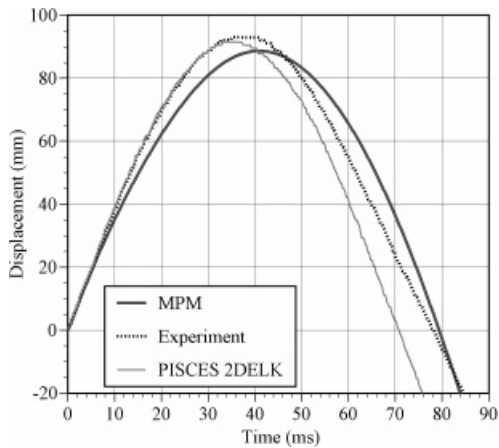
Figure 17. Displacement results for
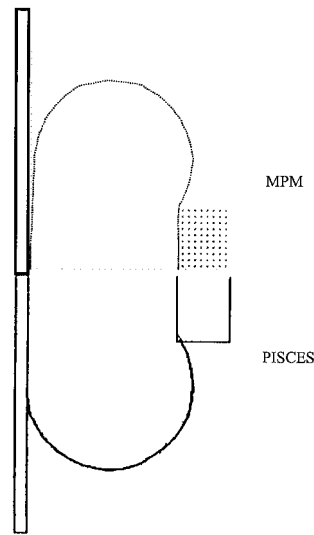the cylindrical probe.

Figure 18. Comparison of PISCES and MPM
deformed configuration for $t = 40$ ms.

force in the solution. In principle, this method would be equivalent to that described above, but would have the advantage of not interfering with the gas particles.

5. CONCLUSIONS

The material point method uses Lagrangian material points and an Eulerian or spatial mesh to define the computational domain. The material points move through the Eulerian mesh, on which the momentum equation is solved. A review of the equations is given as they are developed for general solid materials, membranes and compressible fluids. This paper presents the modifications necessary to simulate the interaction of thin membranes and compressible fluids.

Several test problems are presented to demonstrate the methodology. A fluid-only shock tube problem is used to test the compressible fluid model, and a one-dimensional piston-container problem validates the implementation of fluid–membrane interactions. Both of these problems have analytical solutions that are used for comparison with the numerical results. Two more complex simulations of a gas-filled pressurized membrane and of a probe impacting a pre-inflated airbag show the potential of the method. These last two problems are two dimensional and involve complicated geometry that is easily represented by the material points. In addition, the airbag problem has also been solved using finite elements and experimental measurements have been made, both of which compare well with the MPM results.

The treatment of the interface between the fluid and membrane is simple in the MPM and avoids the time-consuming computations necessary in many methods. One major advantage to this approach is that meshing bodies is trivial. Since points only have to be identified that are inside a body or on membrane surface, the potentially expensive process of meshing with

standard finite elements is avoided. Other advantages are that the constitutive equations are easily changed, and the algorithm runs on a PC or workstation, but can be easily parallelized for more powerful machines and larger problems.

REFERENCES

1. McMaster WH. Computer codes for fluid-structure interactions. *Proceedings 1984 Pressure Vessel and Piping Conference*, San Antonio, TX, June 1984, *UCRL-89724* preprint, Lawrence Livermore National Laboratory, 1984.
2. Buijk AJ, Low TC. Significance of gas dynamics in airbag simulations. *Presented at the 26th ISATA*, Aachen, Germany, September 1993.
3. Buijk AJ, Florie CJL. Inflation of folded driver and passenger airbags. *Presented at the 1991 MSC World Users Conference, Paper 91-04-B,* Los Angeles, California, March 1991.
4. Koivurova H, Pramila A. Nonlinear vibration of axially moving membrane by finite element method. *Computational Mechanics* 1997; **20**:573–581.
5. Nieboer JJ, Wismans J, de Coo PJA. Airbag modeling techniques. *Proceedings of the 34th Stapp Car Crash Conference, SAE Paper 902322*, 1990.
6. Liu WK, Ma DC. Computer implementation aspects for fluid–structure interaction problems. *Computer Methods in Applied Mechanics and Engineering* 1981; **31**:129–148.
7. Nomura T. ALE finite element calculations of fluid-structure interaction problems. *Computer Methods in Applied Mechanics* 1994; **112**:291–308.
8. Brackbill JU, Ruppel HM. FLIP: a method for adoptively zoned, particle-in-cell calculations in two dimensions. *Journal of Computational Physics* 1986; **65**:314–343.
9. Brackbill JU, Kothe DB, Ruppel HM. FLIP: a low-dissipation, particle-in-cell method for fluid flow. *Computer Physics Communications* 1988; **48**:25–38.
10. Sulsky D, Chen Z, Schreyer HL. A particle method for history-dependent materials. *Computer Methods in Applied Mechanics and Engineering* 1994; **118**:179–196.
11. Sulsky D, Zhou S-J, Schreyer HL. Application of a particle-in-cell method to solid mechanics. *Computer Physics Communications* 1995; **87**:136–252.
12. Sulsky D, Schreyer HL. Axisymmetric form of the material point method with applications to upsetting and Taylor impact problems. *Computer Methods in Applied Mechanics and Engineering* 1996; **139**:409–429.
13. York AR, Sulsky DL, Schreyer HL. The material point method for simulation of thin membranes. *International Journal for Numerical Methods in Engineering* 1999; **44**:1429–1456.
14. Huerta A, Liu WK. Large-amplitude sloshing with submerged blocks. *Journal of Pressure Vessel Technology* 1990; **112**:104-1-8.
15. Thematic Issue on Particle Simulation Methods, *Computer Physics Communications* 1995; **87**(1–2).
16. Special Issue on Meshless Methods, *Computer Methods in Applied Mechanics and Engineering* 1996; **139**(1–4).
17. Peskin CS. Numerical analysis of blood flow in the heart. *Journal of Computational Physics* 1977; **25**:220–252.
18. Peskin CS, McQueen DM. A general method for the computer simulation of biological systems interacting with fluids. *Symposium-Society for Experimental Biology*, U.K., ISSN/ISBN 0081-1386, 1995.
19. LeVeque RJ, Li Z. Immersed interface methods for Stokes flow with elastic boundaries or surface tension. *SIAM Journal on Scientific Computing* 1997; **18**:709–735.
20. Jones AV. Fluid-structure coupling in Lagrange–Lagrange and Euler–Lagrange descriptions. *Report EUR 7424 EN*, Nuclear Science and Technology, Commission of the European Communities, Joint Research Centre, Ispra Establishment, Italy, 1981.
21. Neishlos H, Israeli M, Kivity Y. Stability of some explicit difference schemes for fluid–structure interaction problems. *Computers and Structures* 1981; **13**:97–101.
22. Neishlos H, Israeli M, Kivity Y. The stability of explicit difference schemes for solving the problem of interaction between a compressible fluid and an elastic shell. *Computer Methods in Applied Mechanics and Engineering* 1983; **41**:129–143.
23. Burgess D, Sulsky D, Brackbill JU. Mass matrix formulation of the FLIP particle-in-cell method. *Journal of Computational Physics* 1992; **103**:1–15.

24. Bardenhagen SG, Brackbill JU, Sulsky DL. The material-point method for granular material. *Computer Methods in Applied Mechanics and Engineering* 1999; to appear.
25. Wilkins ML. Use of artificial viscosity in multidimensional fluid dynamic calculations. *Journal of Computational Physics* 1980; **36**:281–303.
26. Sod GA. A survey of several finite difference methods for systems of nonlinear hyperbolic conservation laws. *Journal of Computational Physics* 1978; **27**:1–31.
27. Olson LG, Bathe K. A study of displacement-based fluid finite elements for calculating frequencies of fluid and fluid–structure systems. *Nuclear Engineering and Design* 1983; **76**:137–151.
28. de Coo PJA, Nieboer JJ, Wismans J. Computer simulation of driver airbag contact with rigid body. *TNO Report No. 751960020 to MVMA*, December 1989.